Measurement of valence-band offsets of InAlN/GaN heterostructures grown by metal-organic vapor phase epitaxy

M. Akazawa,[1,2,a)] B. Gao,[1] T. Hashizume,[1,2] M. Hiroki,[3] S. Yamahata,[3] and N. Shigekawa[3]
[1]*Research Center for Integrated Quantum Electronics, Hokkaido University, Sapporo 060-8628, Japan*
[2]*JST-CREST, Sanbancho, Chiyoda-ku, Tokyo, 102-0075, Japan*
[3]*NTT Photonics Laboratories, NTT Corporation, Atsugi, Kanagawa 243-0198, Japan*

(Received 3 August 2010; accepted 13 November 2010; published online 3 January 2011)

The valence band offsets, ΔE_V, of $In_{0.17}Al_{0.83}N/GaN$, $In_{0.25}Al_{0.75}N/GaN$, and $In_{0.30}Al_{0.70}N/GaN$ heterostructures grown by metal-organic vapor phase epitaxy were evaluated by using x-ray photoelectron spectroscopy (XPS). The dependence of the energy position and the full width at half maximum of the Al $2p$ spectrum on the exit angle indicated that there was sharp band bending caused by the polarization-induced electric field combined with surface Fermi-level pinning in each ultrathin InAlN layer. The ΔE_V values evaluated without taking into account band bending indicated large discrepancies from the theoretical estimates for all samples. Erroneous results due to band bending were corrected by applying numerical calculations, which led to acceptable results. The evaluated ΔE_V values were 0.2 ± 0.2 eV for $In_{0.17}Al_{0.83}N/GaN$, 0.1 ± 0.2 eV for $In_{0.25}Al_{0.75}N/GaN$, and 0.0 ± 0.2 eV for $In_{0.30}Al_{0.70}N/GaN$. Despite the large decrease of around 1.0 eV in the band gap of InAlN layers according to the increase in the In molar fraction, the decrease in ΔE_V was as small as 0.2 eV. Therefore, the change in band-gap discontinuity was mainly distributed to that in conduction band offset. © *2011 American Institute of Physics*.
[doi:10.1063/1.3527058]

I. INTRODUCTION

Group III-nitrides and their alloys are promising materials that should enable excellent high-power, high-frequency, and optoelectronic devices to be fabricated. Their heterostructures can provide a high-density two-dimensional electron gas (2DEG) with a high saturation velocity in wide-gap semiconductors. Lattice-matched $In_xAl_{1-x}N$ ($x = 0.17-0.18$)/GaN heterostructures without doping can especially provide a 2DEG with high density exceeding 2×10^{13} cm^{-2},[1–8] due to the difference in spontaneous polarization at the interface.[9] High-performance InAlN/GaN high-electron mobility transistors (HEMTs) have actually been fabricated and reported.[2,3,5,10] If we expand the scope to include nonlattice-matched InAlN/GaN heterostructures, the band gap, E_g, of InAlN can be greatly changed from 6.2 eV (AlN) to 0.67 eV (InN).[11] It has theoretically been predicted that the decrease in the conduction band offset, ΔE_C, according to the increase in the In molar fraction is much larger than decrease in the valence band offset, ΔE_V.[12] This interface property is useful for barrier-height engineering. The large change in ΔE_C according to the molar fraction can be verified by confirming the small change in ΔE_V. However, there have been no reports on measuring the change in ΔE_V by changing the molar fraction.

One of the most useful methods of investigating ΔE_V is by applying x-ray photoelectron spectroscopy (XPS) to the interface between ultrathin InAlN and GaN layers. However, evaluating ΔE_V by using XPS is possibly erroneous due to sharp band bending caused by the spontaneous and piezoelectric polarization in ultrathin InAlN layers. In our preliminary work,[13] the ΔE_V of lattice-matched $In_{0.17}Al_{0.83}N/GaN$ grown by metal-organic vapor phase epitaxy (MOVPE) was evaluated correctly by taking into account band bending due to the polarization-induced electric field combined with surface Fermi-level pinning. In addition to the lattice-matched $In_{0.17}Al_{0.83}N/GaN$ heterostructure, the pseudomorphic heterostructures of $In_{0.25}Al_{0.75}N/GaN$ and $In_{0.30}Al_{0.70}N/GaN$ were also grown and characterized in this work. Erroneous results due to band bending in ultrathin InAlN layers were corrected by applying numerical calculations. Using the measured peak positions of core levels, E_{CL}'s, without correction, the evaluated ΔE_V values deviated from the theoretical estimates according to Refs. 11 and 12. However, the corrected values for all the InAlN/GaN interfaces were in good agreement with the theoretical estimates. Despite the large decrease in E_g of the InAlN layers according to the increase in the In molar fraction, small decrease in ΔE_V were evaluated at the InAlN/GaN interfaces. Therefore the decrease in E_g discontinuity was mostly distributed to that in ΔE_C at the InAlN/GaN interfaces.

II. EXPERIMENTAL

The sample structure used to investigate the interface with XPS is schematically shown in Fig. 1. All the samples were grown on sapphire (0001) substrates by MOVPE without any doping. $In_{0.17}Al_{0.83}N/GaN$, $In_{0.25}Al_{0.75}N/GaN$, and $In_{0.30}Al_{0.70}N/GaN$ heterostructures with 2.5 nm-thick InAlN layers were prepared. Here, we have defined the photoelectron exit angle, θ, as the elevation angle indicated in Fig. 1. To measure bulk material constants, thick (around 15 nm) $In_{0.17}Al_{0.83}N$, $In_{0.25}Al_{0.75}N$, and $In_{0.30}Al_{0.70}N$ layers on GaN and a 2 μm-thick GaN single layer were also prepared. Tri-

a)Electronic mail: akazawa@rciqe.hokudai.ac.jp.

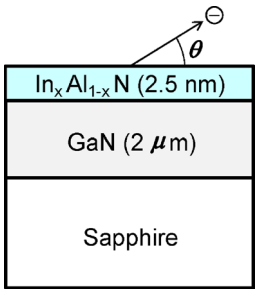

FIG. 1. (Color online) Sample structure for XPS investigations. Definition of exit angle θ is also shown.

methylgallium was used as a precursor for gallium, trimethylaluminum for aluminum, trimethylindium for indium, and ammonia for nitrogen. The growth temperature was set at 1000 °C for GaN, 820 °C for $In_{0.17}Al_{0.83}N$, 780 °C for $In_{0.25}Al_{0.75}N$, and 730 °C for $In_{0.30}Al_{0.70}N$. The details on the growth conditions are described in Ref. 6. Successful control of the molar fraction in MOVPE growth was confirmed for the thick InAlN layers by using x-ray diffraction. XPS was done by using a monochromated Al $K\alpha$ x-ray source (1486.6 eV). The binding energy was calibrated by adjusting the peak positions of the C 1*s* core levels to 285.0 eV for each sample surface. The morphology of the surfaces was investigated by atomic force microscopy. The surfaces of all the heterostructure samples with the ultrathin InAlN layers were smooth, having monolayer steps, which indicated that the thin InAlN layer had uniform thickness as a result of layer-by-layer growth. The XPS data also indicated this state. Surface oxide layers were removed by pretreating them with hydrofluoric (HF) acid.

III. THEORY OF MEASUREMENT

A schematic band diagram for the principle of measuring ΔE_V at the InAlN/GaN interface is outlined in Fig. 2, where E_C is the conduction-band minimum, E_V is the valence-band maximum (VBM), and E_F indicates Fermi level that is set to the origin of binding energy in XPS measurement. In our preliminary work,[13] we used the In 4*d* spectrum that overlapped with the Ga 3*d* and N 2*s* spectra very closely on both sides. The Al 2*p* spectrum, however, does not overlapped with any other spectra and is therefore more suitable

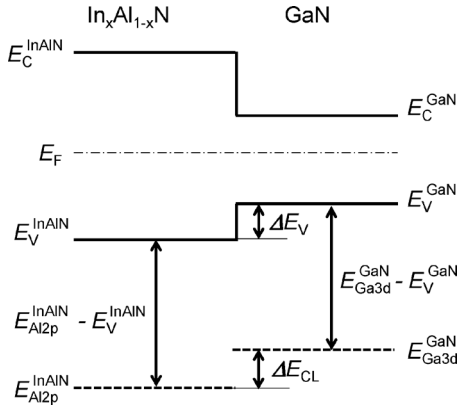

FIG. 2. Schematic band diagram for XPS measurement of ΔE_V.

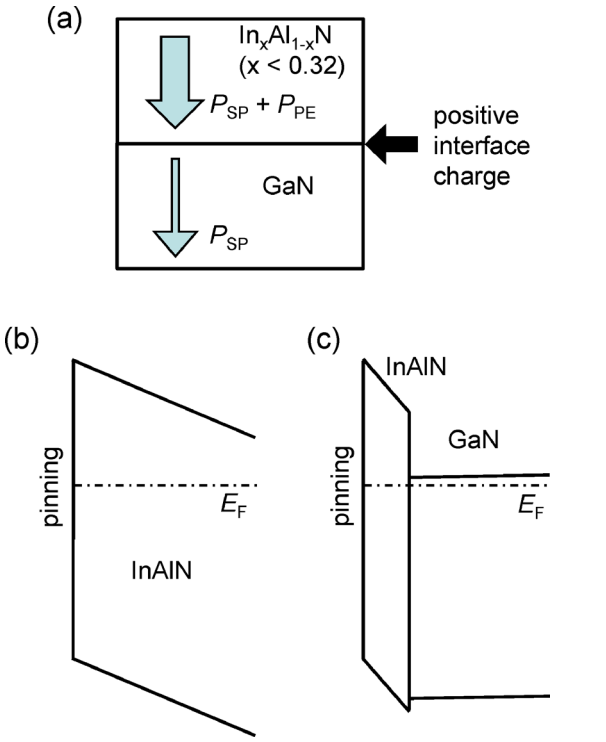

FIG. 3. (Color online) (a) Polarization in pseudomorphic grown wurtzite InAlN/GaN heterostructure with Ga-face polarity. (b) and (c) show possible sharp band bending, in the range of probing depth, schematically for thick and thin InAlN samples.

for the ΔE_V measurement. We therefore used Al 2*p* in the present work. The ΔE_V can be estimated from[14]

$$\Delta E_V = \Delta E_{CL} + (E_{Ga\ 3d}^{GaN} - E_V^{GaN}) - (E_{Al\ 2p}^{InAlN} - E_V^{InAlN}), \quad (1)$$

where $\Delta E_{CL} = (E_{Al\ 2p}^{InAlN} - E_{Ga\ 3d}^{GaN})$ is the binding energy difference between the measured Al 2*p* and Ga 3*d* core-level spectra of the InAlN(2.5 nm)/GaN sample. The two $(E_{CL}^{material} - E_V^{material})$ terms represent the difference in binding energies between the core level and the VBM for GaN and InAlN as bulk material constants. Here, the E_g of InAlN is larger than that of GaN in the range of the molar fraction of the prepared samples.[11,12] The band alignment is therefore type II when $\Delta E_V < 0$. This method can, however, be applied to a sample in a nearly flat-band situation, with negligible band bending, at the surface to depths of around 10 nm. This situation will be referred to as a "quasiflat-band" situation after this. If there is sharp band bending at the sample surfaces that affects the XPS data, correction is needed for E_{CL}'s.

In pseudomorphic grown wurtzite $In_xAl_{1-x}N$ ($x < 0.32$)/GaN heterostructures with Ga-face polarity, the sum of spontaneous polarization, P_{SP}, and piezoelectric polarization, P_{PE}, in InAlN is larger than P_{SP} in GaN as illustrated in Fig. 3(a).[7] This difference in polarization at the heterointerface produces positive interface charge. Since the Fermi level should be pinned at the InAlN surface, sharp band bending can occur in the InAlN layer. Figures 3(b) and 3(c) show the schematics for the possible surface band bending in the range of the probing depth for samples with thick and ultrathin InAlN layers. Uniform internal electric fields in the outer InAlN layers were calculated for all the samples in the

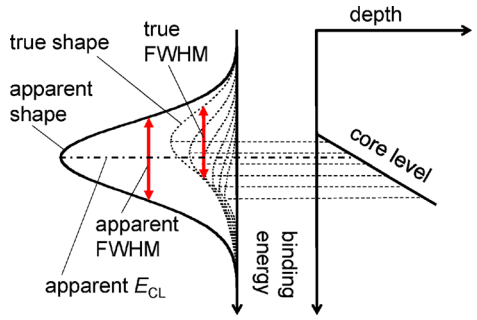

FIG. 4. (Color online) Schematic explaining increases in E_{CL} and FWHM in apparent spectrum.

range of probing depths and observed surface potentials that will be described later, while the nonuniform electric fields were calculated for GaN layers. Similar results have previously been reported.[6–8] In XPS measurement, only shallow parts of InAlN layers were probed as shown in Fig. 3(b) for the samples with thick InAlN layers with 2DEG, resulting in no detection of the Ga $3d$ spectrum from the host GaN layer. The samples with ultrathin InAlN layers were without 2DEG, which was confirmed by the contactless eddy current method. Consequently, the band bending in the GaN layers of the samples with ultrathin InAlN layers would be observed as a slight tilt of the potential or a nearly flat band in the range of the probing depth. For example, Fig. 3(c) indicates the observed result, for the $In_{0.17}Al_{0.83}N$ (2.5 nm)/GaN sample, that will be described in Sec. IV. A normally-off type GaN-based HEMT has recently been fabricated by using an ultrathin $In_{0.17}Al_{0.83}N$ (1 nm)/AlN (1 nm) barrier,[10] which supports our results because the barrier thickness and the sum of interface charges[8] are close to those of the $In_{0.17}Al_{0.83}N$ (2.5 nm)/GaN sample.

In the situations shown in Figs. 3(b) and 3(c), the core levels in the InAlN layer are also bent along with the valence band. As schematically outlined in Fig. 4, the observed spectrum is given by integrating the true spectrum from each depth point along the bent core level. Therefore, sharp band bending results in apparent increases in E_{CL} and the full width at half maximum (FWHM) of core-level spectra from the InAlN layer. This phenomenon becomes more remarkable by increasing θ to extend the probing depth. Furthermore, the E_{CL} of the core-level spectra from the GaN layer increases due to the total potential drop in the InAlN layer for the InAlN/GaN heterostructure sample. With the band bending in Fig. 3(c), ΔE_V might be evaluated to have a negative value despite the type-I alignment. Therefore, we have to derive the actual E_{CL}'s by subtracting increases due to band bending so that we can correctly evaluate ΔE_{CL}.

The sequence of correction for ΔE_V at the InAlN/GaN heterointerfaces involves three steps

(1) The internal electric field in InAlN is extracted. Assuming a uniform internal electric field in the InAlN layer, the band bending for the entire heterostructure including the GaN layer is calculated by solving the Poisson equation using the measured surface Fermi level, E_{Fsurf}, position as the boundary condition for strong pinning. Then, the apparent E_{CL} and FWHM due to band bending are calculated for Al $2p$ and Ga $3d$. This procedure is repeated to find the most suitable internal electric field in InAlN that achieves the apparent E_{CL} and FWHM observed for Al $2p$ and Ga $3d$.
(2) E_{CL} values are corrected for Al $2p$ and Ga $3d$ by subtracting the apparent increases due to band bending to correctly evaluate the ΔE_{CL} value.
(3) ΔE_V is derived using the corrected ΔE_{CL} value in Eq. (1).

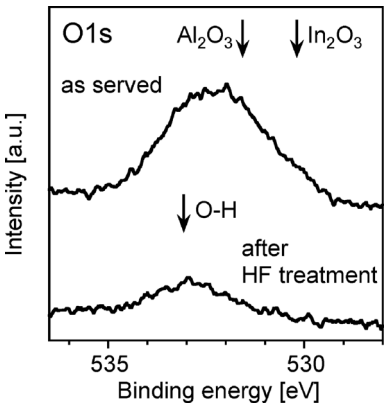

FIG. 5. XPS O $1s$ spectra observed for $In_{0.17}Al_{0.83}N$ layer.

The details on the calculations to estimate the apparent E_{CL} and FWHM of core-level spectra due to band bending are as follows. A core-level spectrum as a function of the binding energy, E, from a layer of thickness d is given by[15]

$$I(E) = \int_0^d I_0(E,z)\exp\left(-\frac{z}{\lambda}\right)dz, \tag{2}$$

where z, λ, and $I_0(E,z)$ correspond to the depth from the surface, the escape depth of the photoelectrons, and the spectrum generated at each depth point. Here, to do the calculations within a practical time frame and to avoid heavy computation, the $I_0(E,z)$ for one spin orbital is represented by the pseudo-Voigt function given by

$$V(E,z) = I_{00}\left[\alpha\exp\left\{-\ln 2\frac{(E-E_0)^2}{(F/2)^2}\right\} + (1-\alpha)\frac{1}{1+\left\{-\frac{(E-E_0)^2}{(F/2)^2}\right\}}\right], \tag{3}$$

where I_{00}, α, E_0, and F are the intensity, the ratio of the Gaussian function, the binding energy of the core level, and the actual FWHM. When surface band bending is not negligible on the scale of the escape depth of photoelectrons, E_0 should be treated as a function of depth z to be $E_0(z)$. The F was assumed to be a sample dependent constant. The α was fixed to 0.73 for both Al $2p$ and Ga $3d$ spectra. For Al $2p$ and Ga $3d$ spectra, $I_0(E,z)$ is given by a weighted combination of two pseudo-Voigt-function components taking into account the spin-orbit splitting of 0.41 eV for Al $2p$ and

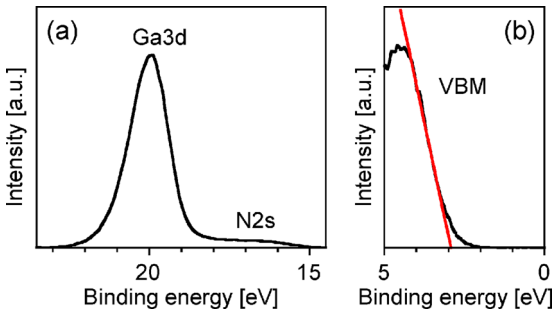

FIG. 6. (Color online) XPS Ga $3d$ and VBM spectra obtained for thick GaN sample.

0.44 eV for Ga $3d$.[16] Furthermore, λ can be changed by changing θ according to

$$\lambda = \lambda_0 \sin \theta, \tag{4}$$

where λ_0 indicates the inelastic mean free path of a photoelectron. The value of λ_0 was calculated using a previously reported equation[17,18] that was demonstrated to fit the experimental data for several materials including GaN.[19] The λ_0 of Al $2p$ spectrum was calculated to be 2.87 nm for $In_{0.17}Al_{0.83}N$, 2.79 nm for $In_{0.25}Al_{0.75}N$, and 2.76 nm for $In_{0.30}Al_{0.70}N$. The λ_0 of Ga $3d$ spectrum was calculated to be 2.58 nm for GaN, 2.95 nm for $In_{0.17}Al_{0.83}N$, 2.88 nm for $In_{0.25}Al_{0.75}N$, and 2.84 nm for $In_{0.30}Al_{0.70}N$.

IV. RESULTS AND DISCUSSION

A. Measurement of bulk material constants

We found that HF treatment efficiently removed oxides from the InAlN and GaN surfaces. Figure 5 shows the O $1s$ spectra before and after HF treatment for $In_{0.17}Al_{0.83}N$ at $\theta = 45°$. In_2O_3 component appear at 530.2 eV (Ref. 20) and that for Al_2O_3 appear at 531.6 eV.[21] The spectral intensity at these binding energies drastically decreased after HF treatment leaving only a faint component assigned to O–H bonding.[22] Similar results were also obtained for the $In_{0.25}Al_{0.75}N$, $In_{0.30}Al_{0.70}N$, and GaN surfaces.

The Ga $3d$ and VBM spectra observed at $\theta = 45°$ for the HF-treated thick GaN layer on a sapphire substrate are shown in Fig. 6. The efficiency of HF treatment can also be seen here. The shape of the Ga $3d$ spectrum was identical to that obtained for the GaN (2×2) clean surface grown by molecular beam epitaxy, which indicated that the surface was nearly oxide free. The VBM position was determined by linear extrapolation of the low binding energy edge of the valence band spectrum. The value of $(E_{\mathrm{Ga\ 3d}}^{\mathrm{GaN}} - E_{\mathrm{V}}^{\mathrm{GaN}})$ was evaluated to be 17.10 ± 0.07 eV. The same value was also obtained for the thick GaN layer on an SiC substrate.

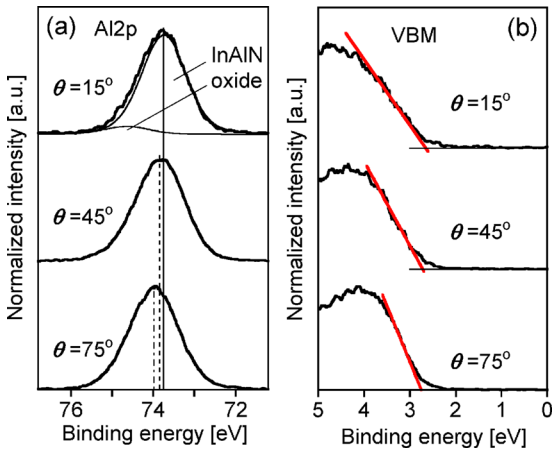

FIG. 7. (Color online) XPS Al $2p$ and VBM spectra obtained for $In_{0.17}Al_{0.83}N$ (14.5 nm)/GaN heterostructure.

Figures 7(a) and 7(b) show the Al $2p$ and VBM spectra obtained at three different θ's for the thick $In_{0.17}Al_{0.83}N$ samples. No oxide components were detected for Al $2p$ spectra at $\theta = 45°$ or 75°, even though they were detected at the surface sensitive angle of $\theta = 15°$. It can be seen that the Al $2p$ spectrum shifts to higher binding energies with the increase in θ, which indicates that there was sharp band bending in the $In_{0.17}Al_{0.83}N$ layer. We also found that the FWHM of the Al $2p$ spectrum increased with θ. The results are summarized in Table I with the values calculated by assuming an internal electric field of 1.2 MV/cm in the $In_{0.17}Al_{0.83}N$ layer. Note that the corrected VBM position in Table I is close to that reported for $In_{0.16}Al_{0.84}N$.[23] Consequently, the bulk material constant $(E_{\mathrm{Al\ 2}p}^{\mathrm{InAlN}} - E_{\mathrm{V}}^{\mathrm{InAlN}})$ was determined to be 71.10 ± 0.07 eV for $In_{0.17}Al_{0.83}N$. The same value was also obtained for the thick $In_{0.25}Al_{0.75}N$ layer by applying the same method. However, applying the same method to the thick $In_{0.30}Al_{0.70}N$ layer did not lead to an acceptable result. The thickness needed to investigate the bulk material constant was probably too large for the $In_{0.30}Al_{0.70}N$ layer to maintain good bulk quality. (Precise evaluation of the critical thickness was beyond the scope of this work.) Therefore, the value of $(E_{\mathrm{Al\ 2}p}^{\mathrm{InAlN}} - E_{\mathrm{V}}^{\mathrm{InAlN}})$ for $In_{0.30}Al_{0.70}N$ was extrapolated from the results of two other samples to be 71.10 eV.

B. Measurement of band offsets

To determine ΔE_{V}, the ΔE_{CL} between Al $2p$ and Ga $3d$ spectra was measured for each heterostructure with the thin

TABLE I. Summary of measured and calculated values of E_{CL} and FWHM for thick $In_{0.17}Al_{0.83}N$ layer.

	$E_{\mathrm{Al\ 2}p}$ (eV)			FWHM of Al $2p$ (eV)			VBM (eV)		
		Calculated			Calculated			Calculated	
θ	Measured	Apparent	Corrected	Measured	Apparent	Corrected	Measured	Apparent	Corrected
15°	73.75	73.75	73.66	1.28	1.29	1.28	2.65	2.63	2.54
45°	73.87	73.87	73.66	1.40	1.38	1.28	2.72	2.74	2.54
75°	73.98	73.95	73.66	1.42	1.44	1.28	2.75	2.75	2.54

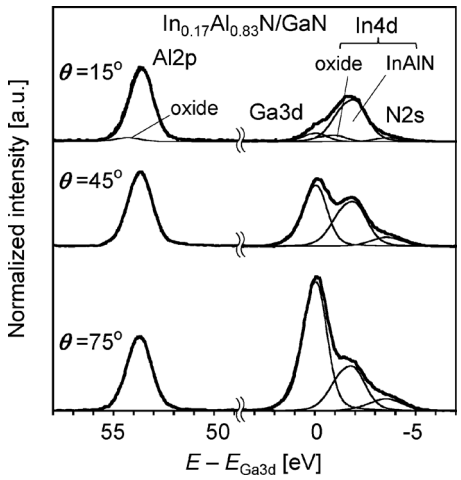

FIG. 8. XPS Al $2p$, Ga $3d$, In $4d$, and N $2s$ core-level spectra obtained for $In_{0.17}Al_{0.83}N$ (2.5 nm)/GaN heterostructure.

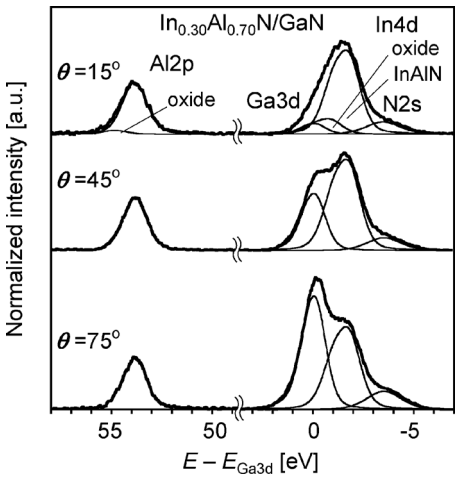

FIG. 10. XPS Al $2p$, Ga $3d$, In $4d$, and N $2s$ core-level spectra obtained for $In_{0.30}Al_{0.70}N$ (2.5 nm)/GaN heterostructure.

(2.5 nm) InAlN top layer. The spectra we obtained are shown in Fig. 8 for the lattice-matched $In_{0.17}Al_{0.83}N/GaN$ heterostructure, in Fig. 9 for the pseudomorphic $In_{0.25}Al_{0.75}N/GaN$ heterostructure, and in Fig. 10 for the pseudomorphic $In_{0.30}Al_{0.70}N/GaN$ heterostructure. The measured values of ΔE_{CL} and ΔE_V without correction have been summarized in Table II. Using the previously mentioned bulk constant values, all the ΔE_V values were evaluated to be negative and were not independent of θ. The evaluated ΔE_V values in Table II are also plotted in Fig. 11 to compare them with the calculated values according to Refs. 11 and 12. The ΔE_V values without correction deviated from the calculated values and indicated type-II alignments for all the samples despite the prediction of type-I alignments. In addition, the E_{CL} and FWHM of the Al $2p$ spectra for $In_{0.17}Al_{0.83}N/GaN$ and $In_{0.25}Al_{0.75}N/GaN$ interfaces increased with increasing θ as summarized in Table III. These results indicate that there was sharp band bending in the ultrathin InAlN layers again. Here, the detected internal electric field decreased according to the increase in the In molar fraction. The observed trend is in agreement with the theoretical estimates.[9]

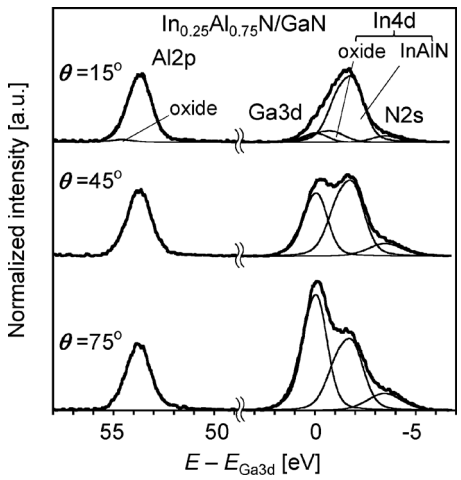

FIG. 9. XPS Al $2p$, Ga $3d$, In $4d$, and N $2s$ core-level spectra obtained for $In_{0.25}Al_{0.75}N$ (2.5 nm)/GaN heterostructure.

For the $In_{0.17}Al_{0.83}N/GaN$ and $In_{0.25}Al_{0.75}N/GaN$ samples, increases in the E_{CL} and FWHM of the Al $2p$ spectra were sufficiently large to extract the internal electric field in the InAlN layers. The previously mentioned calculation reproduced the observed phenomenon for Al $2p$ in the range of experimental error as is also summarized in Table III. The assumed internal electric fields were 3.2 MV/cm for the $In_{0.17}Al_{0.83}N$ layer and 2.4 MV/cm for the $In_{0.25}Al_{0.75}N$ layer. For Ga $3d$ spectra, we found that the apparent shift in $E_{Ga\ 3d}$ due to band bending in GaN was a few tens of millielectron volts for the $In_{0.17}Al_{0.83}N/GaN$ sample and negligible for the other samples. The corrected ΔE_V values were 0.2 eV for $In_{0.17}Al_{0.83}N/GaN$ and 0.1 eV for $In_{0.25}Al_{0.75}N/GaN$, as listed in Table IV with the corrected values of ΔE_{CL}. The measured band alignments for the quasiflat-band situation using the reported E_g values[11] are summarized in Figs. 12(a) and 12(b) for the $In_{0.17}Al_{0.83}N/GaN$ and $In_{0.25}Al_{0.75}N/GaN$ interfaces. Note that the resulting E_{Fsurf} position for the $In_{0.17}Al_{0.83}N$ layer in Fig. 12(a) is close to the experimental result previously reported for $In_{0.16}Al_{0.84}N$.[23]

For the $In_{0.30}Al_{0.70}N/GaN$ sample, however, no large increases depending on θ were observed in either the $E_{Al\ 2p}$ or FWHM as summarized in Table III. Nevertheless, piezoelectric polarization did not completely compensate for spontaneous polarization in the pseudomorphic $In_{0.30}Al_{0.70}N$ layer

TABLE II. Summary of measured results without correction for InAlN/GaN interfaces.

x	θ	ΔE_{CL} (eV)	ΔE_V (eV)
0.17	15°	53.61	−0.4
	45°	53.71	−0.3
	75°	53.74	−0.3
0.25	15°	53.70	−0.3
	45°	53.75	−0.3
	75°	53.78	−0.2
0.30	15°	53.85	−0.2
	45°	53.85	−0.2
	75°	53.85	−0.2

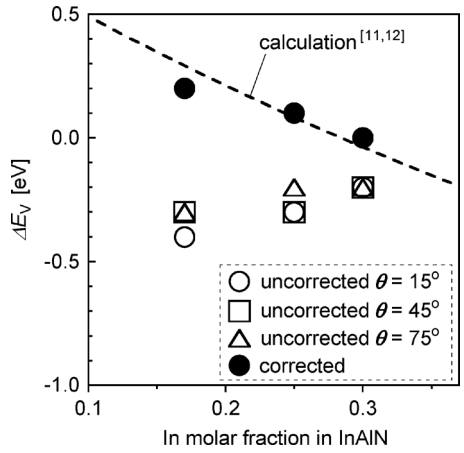

FIG. 11. Measured ΔE_V values with and without correction vs. In molar fraction in comparison with theoretical calculation according to Refs. 11 and 12.

according to the theoretical estimate in Ref. 9. Therefore, it is likely there was an internal electric field in the $In_{0.30}Al_{0.70}N$ layer. The numerical calculations indicated that the increases in apparent $E_{Al\ 2p}$ and FWHM were negligible within experimental error with internal electric fields up to 1.2 MV/cm in the $In_{0.30}Al_{0.70}N$ layer. This maximum value for the electric field is in good agreement with the theoretical estimates in Ref. 9 and leads to the correction of ΔE_V at the $In_{0.30}Al_{0.70}N/GaN$ interface to be 0.0 eV as shown in Fig. 12(c) and Table IV. The rationality of this correction is given by resultant E_{Fsurf} positions as follows.

The Fermi-level stabilization energy, E_{Fstab}, has been reported to be an energy position where E_F stabilizes for sufficiently high damage density.[24] The E_{Fstab} lies at 4.9 eV from the vacuum level in all semiconductors.[24] This energy level can therefore be used as a common benchmark point for E_{Fsurf} position. In the quasiflat-band situation of InAlN/GaN heterointerface, the value of $(E_{Fsurf}-E_{Fstab})$ should be identical for both InAlN and GaN layers. The measured values of $(E_{Fsurf}-E_{Fstab})$ are summarized in Table V. Note that there was 0.2 eV of difference in $(E_{Fsurf}-E_{Fstab})$ between $In_{0.3}Al_{0.7}N$ and GaN without correction for the $In_{0.3}Al_{0.7}N/GaN$ interface, whereas no such differences were

TABLE IV. Summary of corrected ΔE_{CL} and ΔE_V values for InAlN/GaN interfaces.

x	ΔE_{CL} (eV)	ΔE_V (eV)
0.17	54.20	0.2
0.25	54.13	0.1
0.30	54.04	0.0

seen in the corrected data for the $In_{0.17}Al_{0.83}N/GaN$ and $In_{0.25}Al_{0.75}N/GaN$ interfaces. The difference in uncorrected values of $(E_{Fsurf}-E_{Fstab})$ for the $In_{0.30}Al_{0.70}N/GaN$ interface must have been caused by the internal electric field. After correction assuming 1.2 MV/cm in $In_{0.30}Al_{0.70}N$, the difference disappeared, as seen in Table V. Moreover, the dispersion of E_{Fsurf} for the same surface pretreatment for InAlN/GaN heterostructures should be discussed. Even though the E_{Fsurf} positions of the HF-treated samples may disperse statistically depending on the sample, the dispersion for the same treatment is likely to be within a few 0.1 eV. As can be seen from Table V, the $(E_{Fsurf}-E_{Fstab})$ was evaluated to be 0.0 eV for the $In_{0.17}Al_{0.83}N/GaN$ interface and −0.2 eV for the $In_{0.25}Al_{0.75}N/GaN$ interface. For the $In_{0.3}Al_{0.7}N/GaN$ sample, however, the value was estimated to be 0.3 eV for the GaN surface without correction resulting in a wide dispersion of 0.5 eV. This discrepancy dependent on the sample is not acceptable. After correction assuming 1.2 MV/cm in $In_{0.30}Al_{0.70}N$, the dispersion width reduced to be an acceptable value of 0.2 eV. Therefore, correction resulting in a ΔE_V value of 0.0 eV for $In_{0.30}Al_{0.70}N$ was appropriate.

As can be seen in Fig. 11, the corrected ΔE_V values are in good agreement with the calculated values for all the interfaces. The experimental error was evaluated by considering the fitting errors and the discrepancy between repeated measurements to be ±40 meV for ΔE_{CL} and ±70 meV for the two $(E_{CL}-E_V)$ components in Eq. (1). Without correction by using numerical calculations, the total error for ΔE_V is ±180 meV. Fitting by numerical calculations introduces an additional error of ±60 meV resulting in a total error of ±240 meV. Since the final results were approximated values in units of 0.1 eV, the errors in both cases should be ±0.2 eV,

TABLE III. Comparison of measured and calculated values for $E_{Al\ 2p}$ and FWHM of Al 2*p* spectra from ultrathin InAlN layers on GaN.

		$E_{Al\ 2p}$ (eV)			FWHM of Al 2*p* (eV)		
			Calculated			Calculated	
x	θ	Measured	Apparent	Corrected	Measured	Apparent	Corrected
0.17	15°	74.01	74.00	73.80	1.36	1.35	1.28
	45°	74.11	74.11	73.80	1.40	1.40	1.28
	75°	74.13	74.14	73.80	1.41	1.41	1.28
0.25	15°	73.69	73.68	73.52	1.40	1.41	1.36
	45°	73.74	73.76	73.52	1.43	1.43	1.36
	75°	73.77	73.77	73.52	1.44	1.44	1.36
0.30	15°	73.70	73.69	73.61	1.42	1.42	1.41
	45°	73.72	73.73	73.61	1.42	1.42	1.41
	75°	73.73	73.74	73.61	1.42	1.42	1.41

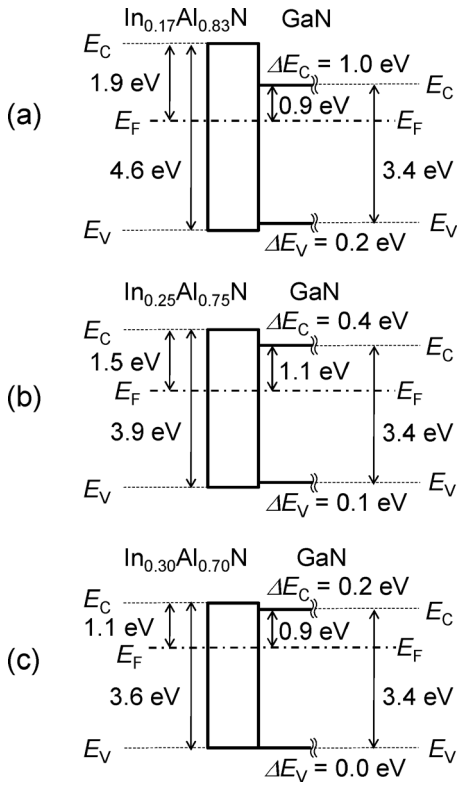

FIG. 12. Schematic band alignments using measured ΔE_V values and reported E_g values (Ref. 11), for (a) $In_{0.17}Al_{0.83}N/GaN$, (b) $In_{0.25}Al_{0.75}N/GaN$, and (c) $In_{0.30}Al_{0.70}N/GaN$ interfaces in quasiflat-band situation.

which is a typical value for the XPS measurements of ΔE_V.[25–28] Even though the evaluated ΔE_V values were small, the E_g of semiconductors on both sides was much larger than the total error. Therefore, the present results provide important information that ΔE_V values are small despite the large band gaps of all samples. The measurement of small ΔE_V values with similar error values can also be found in other reports on TiO_2/GaN $(0.09 \pm 0.25$ eV) (Ref. 27) and HfO_2/GaN $(-0.1 \pm 0.1$ eV) (Ref. 29) interfaces. As can be seen in Fig. 12, the decrease in ΔE_V according to the increase in the In molar fraction should have been much smaller than that in ΔE_C. In other words, the change in E_g discontinuity was mostly distributed to that in ΔE_C at the InAlN/GaN interfaces.

V. CONCLUSION

The ΔE_V of $In_{0.17}Al_{0.83}N/GaN$, $In_{0.25}Al_{0.75}N/GaN$, and $In_{0.30}Al_{0.70}N/GaN$ heterostructures grown by MOVPE were evaluated by using XPS. The E_{CL} and FWHM of the Al $2p$ increased according to the exit angle, which was explained by band bending due to the polarization-induced electric field in ultrathin InAlN layers combined with surface Fermi-level pinning. The ΔE_V values evaluated by the conventional method were in disagreement with the theoretical estimates for all samples. The evaluations were therefore corrected by numerical calculations taking into account band bending, which led to the ΔE_V values being in good agreement with the theoretical estimates for all the interfaces. The evaluated ΔE_V values were 0.2 ± 0.2 eV for $In_{0.17}Al_{0.83}N/GaN$, 0.1 ± 0.2 eV for $In_{0.25}Al_{0.75}N/GaN$, and 0.0 ± 0.2 eV for $In_{0.30}Al_{0.70}N/GaN$, which indicated that the large change in band-gap discontinuity was mostly distributed to that in ΔE_C.

TABLE V. $(E_{Fsurf} - E_{Fstab})$ values for the InAlN(2.5 nm)/GaN heterostructures in quasiflat-band situation.

	$E_{Fsurf} - E_{Fstab}$ (eV)			
	$In_{0.17}Al_{0.83}N/GaN$ (corrected)	$In_{0.25}Al_{0.75}N/GaN$ (corrected)	$In_{0.30}Al_{0.70}N/GaN$	
			Uncorrected	Corrected
InAlN surface	0.0	−0.2	0.1	0.0
GaN surface	0.0	−0.2	0.3	0.0

[1] J. Kuzmik, IEEE Electron Device Lett. **22**, 510 (2001).
[2] M. Higashiwaki and T. Matsui, Jpn. J. Appl. Phys., Part 2 **43**, L768 (2004).
[3] J. Kuzmík, A. Kostopoulos, G. Konstantinidis, J.-F. Carlin, A. Georgakilas, and D. Pogany, IEEE Trans. Electron Devices **53**, 422 (2006).
[4] M. Gonschorek, J.-F. Carlin, E. Feltin, M. A. Py, and N. Grandjean, Appl. Phys. Lett. **89**, 062106 (2006).
[5] J. Xie, X. Ni, M. Wu, J. H. Leach, Ü. Özgür, and H. Morkoç, Appl. Phys. Lett. **91**, 132116 (2007).
[6] M. Hiroki, N. Maeda, and T. Kobayashi, Appl. Phys. Express **1**, 111102 (2008).
[7] M. Gonschorek, J.-F. Carlin, E. Feltin, M. A. Py, N. Grandjean, V. Darakchieva, B. Monemar, M. Lorenz, and G. Ramn, J. Appl. Phys. **103**, 093714 (2008).
[8] L. Ardaravičius, M. Ramonas, J. Liberis, O. Kiprijanovič, A. Matulionis, J. Xie, M. Wu, J. H. Leach, and H. Morkoç, J. Appl. Phys. **106**, 073708 (2009).
[9] O. Ambacher, R. Dimitrov, M. Stutzmann, B. E. Foutz, M. J. Murphy, J. A. Smart, J. R. Shealy, N. G. Weimann, K. Chu, M. Chumbes, B. Green, A. J. Sierakowski, W. J. Schaff, and L. F. Eastman, Phys. Status Solidi B **216**, 381 (1999).
[10] C. Ostermaier, G. Pozzovivo, J.-F. Carlin, B. Basnar, W. Schrenk, Y. Douvry, C. Gaquière, J.-C. DeJaeger, K. Čičo, K. Fröhlich, M. Gonschorek, N. Grandjean, G. Strasser, D. Pogany, and J. Kuzmík, IEEE Electron Device Lett. **30**, 1030 (2009).
[11] R. E. Jones, R. Broesler, K. M. Yu, J. W. Ager III, E. E. Haller, W. Walukiewicz, X. Chen, and W. J. Schaff, J. Appl. Phys. **104**, 123501 (2008).
[12] W. Walukiewicz, S. X. Li, J. Wu, K. M. Yu, J. W. Ager III, E. E. Haller, H. Lu, and W. J. Schaff, J. Cryst. Growth **269**, 119 (2004).
[13] M. Akazawa, T. Matsuyama, T. Hashizume, M. Hiroki, S. Yamahata, and N. Shigekawa, Appl. Phys. Lett. **96**, 132104 (2010).
[14] J. R. Waldrop and R. W. Grant, Appl. Phys. Lett. **68**, 2879 (1996).
[15] D. Briggs and M. P. Seah, *Practical Surface Analysis by Auger and X-ray Photoelectron Spectroscopy* (Wiley, Sussex, 1983).
[16] Y. Sun, P. Pianetta, P.-T. Chen, M. Kobayashi, Y. Nishi, N. Goel, M. Garner, and W. Tsai, Appl. Phys. Lett. **93**, 194103 (2008).
[17] S. Tanuma, C. J. Powell, and D. R. Penn, Surf. Interface Anal. **17**, 927 (1991).
[18] S. Tanuma, C. J. Powell, and D. R. Penn, Surf. Interface Anal. **21**, 165 (1994).
[19] M. Krawczyk, J. Phys.: Conf. Ser. **100**, 042033 (2008).
[20] G. Hollinger, R. Skheyta-Kabbani, and M. Gendry, Phys. Rev. B **49**, 11159 (1994).
[21] F. S. Aguirre-Tostado, M. Milojevic, B. Lee, J. Kim, and R. M. Wallace, Appl. Phys. Lett. **93**, 172907 (2008).
[22] Y.-J. Lin and C.-T. Lee, Appl. Phys. Lett. **77**, 3986 (2000).
[23] P. D. C. King, T. D. Veal, A. Adikimenakis, H. Lu, L. R. Bailey, E. Iliopoulos, A. Georgakilas, W. J. Schaff, and C. F. McConville, Appl. Phys. Lett. **92**, 172105 (2008).
[24] W. Walukiewicz, Physica B **302–303**, 123 (2001).
[25] G. Martin, A. Botchkarev, A. Rockett, and H. Morkoç, Appl. Phys. Lett. **68**, 2541 (1996).

[26]S. W. King, C. Ronning, R. F. Davis, M. C. Benjamin, and R. J. Nemanich, J. Appl. Phys. **84**, 2086 (1998).
[27]P. J. Hansen, V. Vaithyanathan, Y. Wu, T. Mates, S. Heikman, U. K. Mishra, R. A. York, D. G. Schlom, and J. S. Speck, J. Vac. Sci. Technol. B **23**, 499 (2005).
[28]H. S. Craft, R. Collazo, M. D. Losego, S. Mita, Z. Sitar, and J.-P. Maria, J. Appl. Phys. **102**, 074104 (2007).
[29]T. E. Cook, Jr., C. C. Fulton, W. J. Mecouch, R. F. Davis, G. Lucovsky, and R. J. Nemanich, J. Appl. Phys. **94**, 7155 (2003).